



Molecular hydrogen in minerals as a clue to interpret δD variations in the mantle

B. N. Moine ^{1✉}, N. Bolfan-Casanova², I. B. Radu^{1,3}, D. A. Ionov⁴, G. Costin ⁵, A. V. Korsakov⁶, A. V. Golovin^{6,7}, O. B. Oleinikov⁸, E. Deloule⁹ & J. Y. Cottin¹

Trace amounts of water dissolved in minerals affect density, viscosity and melting behaviour of the Earth's mantle and play an important role in global tectonics, magmatism and volatile cycle. Water concentrations and the ratios of hydrogen isotopes in the mantle give insight into these processes, as well as into the origin of terrestrial water. Here we show the presence of molecular H₂ in minerals (omphacites) from eclogites from the Kaapvaal and Siberian cratons. These omphacites contain both high amounts of H₂ (70 to 460 wt. ppm) and OH. Furthermore, their δD values increase with dehydration, suggesting a positive H isotope fractionation factor between minerals and H₂-bearing fluid, contrary to what is expected in case of isotopic exchange between minerals and H₂O-fluids. The possibility of incorporation of large quantities of H as H₂ in nominally anhydrous minerals implies that the storage capacity of H in the mantle may have been underestimated, and sheds new light on H isotope variations in mantle magmas and minerals.

¹Université de Lyon, UJM-Saint-Etienne, UCA, IRD, CNRS, Laboratoire Magmas et Volcans, UMR6524, Saint-Etienne, France. ²Laboratoire Magmas et Volcans, Université Clermont-Auvergne, CNRS UMR 6524, Clermont-Ferrand IRD R 163, France. ³Department of Geological Sciences, University of Cape Town, Rondebosch, Cape Town 7701, South Africa. ⁴Géosciences Montpellier, Université de Montpellier, Montpellier 34095, France. ⁵Department of Earth, Environmental and Planetary Sciences, Rice University, Houston, TX 77005, USA. ⁶Sobolev Institute of Geology and Mineralogy, Siberian Branch Russian Academy of Sciences (SB RAS), Koptiyuga 3, Novosibirsk 630090, Russia. ⁷Novosibirsk State University, Pirogova 2, Novosibirsk 630090, Russia. ⁸Diamond and Precious Metal Geology Institute, SB RAS, Yakutsk 677007, Russia. ⁹CRPG, UMR7358, CNRS, Université de Lorraine, Vandoeuvre-lès-Nancy, France. ✉email: bertrand.moine@univ-st-etienne.fr

Hydrogen (or water in its oxidised form) plays a key role in the evolution, dynamics and habitability of the Earth. Even in minor amounts, it decreases the mechanical strength and melting temperatures of rocks and minerals, properties that govern volcanism and mantle convection. Hydrogen was incorporated into the Earth's interior during its accretion^{1–3} and then evolved through degassing by volcanism and recycling by subduction. It is an ubiquitous trace component of nominally anhydrous minerals (NAMs) in the upper mantle, estimated to amount, as water, to 0.5–1 times the mass of the oceans^{4,5}, with cosmochemical arguments leading to an estimate of up to seven oceanic masses in the initial Bulk Silicate Earth⁶. So far, hydrogen was thought to exist in the mantle in the form of hydroxyl (OH) with storage capacity depending on depth^{7,8}. An equivalent to a few hundred ppm by weight of H₂O was measured in peridotite xenoliths (mantle fragments brought up by volcanic eruptions)^{9,10} and up to 1.2 wt% H₂O in a ringwoodite inclusion in an ultradeep diamond from the transition zone¹¹. On the other hand, the studies of eclogite xenoliths from Slave, West African and Zimbabwe cratons indicate that oxygen fugacity, *f*O₂, ranges from Δlog*f*O₂ –2 to –4.5¹² relative to the Fayalite–Magnetite–Quartz buffer^{13,14}. At such fugacity, a substantial amount of H should be present in a reduced form¹⁵. Reducing conditions were demonstrated experimentally to greatly decrease the solubility of OH in olivine¹⁶ and it was recently discovered that H₂ could also be dissolved in NAMs, while it had remained undetectable due to its low infra-red extinction coefficient¹⁷.

Here we report H concentration, speciation and isotope ratios for omphacite (sodic clinopyroxene) from 12 eclogite xenoliths from the Kaapvaal (Roberts Victor Mine) and Siberian (Obnazhennaya kimberlite) cratons. These eclogites are bi-mineralic (omphacite, garnet) and corundum-bearing rocks (Fig. 1) with estimated equilibrium conditions of 2.1–3.4 GPa, 805–1110 °C, and 2.8–4.1 GPa, 923–1140 °C, respectively (Supplementary Table 1). They are believed to represent subducted oceanic crust preserved in the cratonic root for >2 billion years and unaffected by host kimberlite or older melts¹⁸. The samples were analysed for their hydrogen abundances (expressed as water) and isotopic composition by Thermal Conversion-Elemental Analyser coupled with continuous flow mass spectrometer (TC/EA-IRMS^{19,20}). Hydrogen was also measured in the omphacite by SIMS (Secondary Ion Mass Spectrometry) and FTIR (Fourier Transform Infra-red Spectroscopy). The hydrogen abundances obtained by TC/EA-IRMS and SIMS (that detect all forms of hydrogen) are consistently higher than those obtained by FTIR (that only detects OH and H₂O efficiently), see Table 1. We propose that the

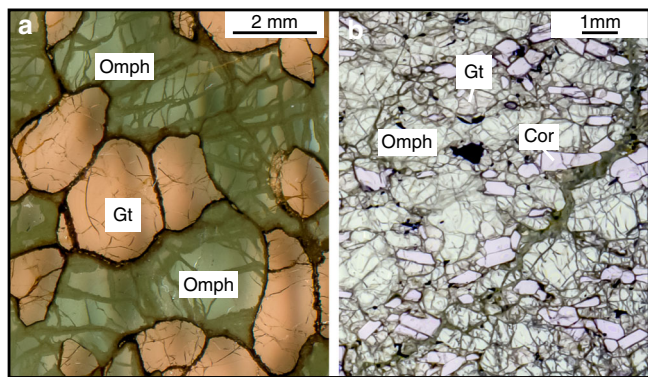


Fig. 1 Thin section images of eclogite samples. **a** biminerallitic eclogite from Roberts Victor Mine (South Africa) and **b** corundum-bearing eclogite from Obnazhennaya kimberlite (Siberia).

Table 1 Water content and hydrogen isotope composition of omphacites.

Sample	<i>n</i>	δD‰ vsMOW	±‰	H ₂ O (ppm)	TC/EA-IRMS	1SD	<i>n</i>	H ₂ O _{tot} (ppm) FTIR	±30%	H ₂ O (ppm) SIMS	1SD	Abs norm 5200 cm ⁻¹	H ₂ O _{mol} (ppm) FTIR 5200 cm ⁻¹	Abs Int norm 4000–4300 cm ⁻¹	H ₂ (ppm)	1SD
Obn108	12	-107	11	2750		100	7	1177	353	4850	340	0.0536	178	4.62	175	41
Obn110	12	-120	11	4850		260	6	1249	375	4850	340	0.0417	138	6.02	400	51
Obn111	9	-116	4	4650		540	9	1413	424	4850	340	0.0425	141	9.42	360	76
Obn112	9	-126	5	5065		340	12	929	279	4850	340	0.0520	172	14.1	460	49
RV179	1	-92		720		120	9	120	36						67	4
RV203	3	-92	2	1315		130										
RV233	5	-99	5	1770		200	9	354	106						157	25
RV360	5	-107	2	2400		300	9	123	37						253	34
RV377	4	-93	3	1040		10										
RV469	3	-99	2	1467		65										
RV488	3	-91	2	1230		280	9	173	52						117	32
RV513	4	-89	3	1256		256	9	255	77						111	30

Water content and H isotopic composition were measured using a Thermal conversion/Elemental Analyser coupled with Isotope-Ratio Mass spectrometer (TC/EA-IRMS). Fourier Transform Infra Red (FTIR) and Secondary Ion Mass Spectrometry (SIMS) analyses. FTIR concentrations were calculated using previously published absorption coefficient¹⁷. Molecular water content was estimated based on the specific IR absorption peak (5200 cm⁻¹) and the absorption coefficient of²⁷. Molecular H₂ was calculated by difference between total H₂O content (TC/EA-IRMS) and FTIR integrated intensity in the range of 3000–3800 cm⁻¹, accounting for both OH and potential H₂O_{molecular}. Abs. norm absorbance corresponding to 5200 cm⁻¹ peak height, 1 SD standard deviation, *n* number of analyses.

“missing” hydrogen undetected by FTIR is stored in minerals as molecular H_2 , which implies that current estimates for total hydrogen in the mantle may be too low. Our results also show that H_2 concentrations are correlated with H isotope compositions, providing new insights into H-isotope systematics in mantle rocks and minerals.

Results and discussion

H contents. The water concentrations (Table 1) in the omphacite measured by TC/EA-IRMS range from 720 to 5065 wt ppm, consistent with data for orogenic (crustal) eclogites (1200–6000 ppm^{21–23}), and are generally much higher than the maximum of 600 ppm H_2O reported previously for mantle pyroxenes^{10,24,25}. Thus, eclogites could represent a significant reservoir of water in the cratonic lithosphere, despite their relatively low average abundance (2%)^{22,23}, as well as generally in the convecting mantle²⁶. FTIR spectra in the OH region (2800–3800 cm^{-1} ; Fig. 2) systematically indicate much lower water contents (100–1500 ppm H_2O) than those obtained by TC/EA-IRMS or SIMS (Table 1). The most important difference between the two methods is that TC/EA-IRMS records the totality of H atoms whereas the FTIR value only relates to structurally bound OH and molecular water²⁷. This suggests that some hydrogen is stored in the omphacite not only as OH but in a different form. Discrepancies between bulk and spectroscopic methods have already been observed for omphacites in orogenic eclogites and magmatic clinopyroxene^{21,28} and tentatively explained by the presence of nano-bubbles^{29,30} of molecular water in the minerals. Although previous work did not identify molecular water spectroscopically, except maybe through the band at 3400 cm^{-1} ³¹, we observed it in some of the analysed grains, albeit with a very noisy signal. Its contribution is very low, 140–290 ppm, within the error of TC/EA-IRMS and FTIR measurements (Table 1), estimated based on the 5200 cm^{-1} specific band³² using published absorbance coefficients²⁷. Molecular water, therefore, cannot account for the measured H excess. It thus looks like most of the total water in minerals measured in the 2800–3800 cm^{-1} range is present in the form of hydroxyl (OH). The SIMS H_2O measurements for sample Obn110 are consistent with TC/EA-IRMS data (4850 ppm, Table 1). Since SIMS is a microbeam technique (that measures all H atoms independently of their speciation), the fact that the water content it provides agrees with the bulk water measurements by TC-EA/IRMS indicates that the amount of H in occasional micro-inclusions and/or fractures is not significant.

H speciation. We also detected a very small and pleochroic peak in the infra-red spectra near 4100 cm^{-1} for the most water-rich omphacites from corundum-bearing Obnazhennaya eclogites that contain 2750–5065 wt ppm water based on the TC/EA-IRMS method (Fig. 2). This peak was previously proposed to correspond to molecular H_2 ¹⁷. Molecular H_2 does not normally respond to infra-red excitation due to its symmetry. However, if H_2 is dissolved in an ionic environment, the weak forces cause the appearance of a dipole interacting with infra-red radiation³³. The centroid of this peak is reduced by ~ 50 cm^{-1} compared with that of molecular H_2 vapour determined by Raman spectroscopy¹⁷. We calculated the amount of molecular H_2 (70–460 wt ppm; Table 1) by difference between the FTIR and TC/EA IRMS data, and found H/OH molar ratios > 3 .

It is further possible to estimate the IR absorption coefficient for H_2 from the FTIR absorbance areas and H_2 contents determined above using the Beer-Lambert law (see “Methods” and Supplementary Fig. 1). The fact that the concentration of molecular H_2 calculated as the difference between bulk water obtained from TC-EA-IRMS and OH obtained from FTIR

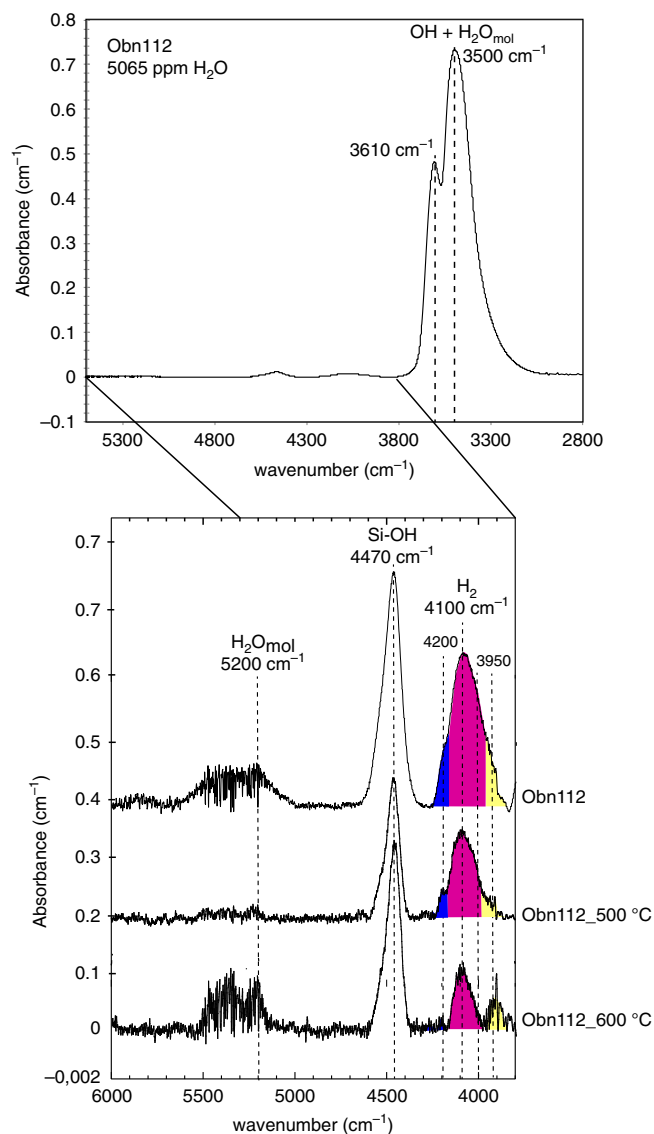


Fig. 2 Unpolarised FTIR spectra of omphacite (Obn112 sample). In the Fourier Transform Infra Red (FTIR) spectra, the 2800–5500 cm^{-1} range show main peaks in the 3000–3800 cm^{-1} range corresponding to OH and molecular H_2O (stretching). Secondary peaks in the 3800–6000 cm^{-1} interval correspond to molecular H_2 (4100 cm^{-1}), Si-OH (4470 cm^{-1}), and molecular water (5200 cm^{-1}). A comparison between unheated and heated samples (500 and 600 °C) shows decreasing intensity of the peak at 4100 cm^{-1} with increasing temperature. The widening of the peak with increasing H_2 content is due to overlapping with two smaller peaks at 4200 and 3950 cm^{-1} . Note that the low intensity of the band at 5200 cm^{-1} related to molecular water indicates negligible fluid inclusion contributions.

correlates positively with the integrated absorbance indicates that the assignment of the 4100 cm^{-1} peak to H_2 is correct. Furthermore, the average linear absorption coefficient of H_2 that we calculate (Table 1) is 1500 times lower than for OH (0.13 ± 0.3 $l mol(H_2)^{-1} cm^{-1}$ or $\sim 44 \pm 10$ $l mol(H_2)^{-1} cm^{-2}$ for H_2 vs. $65,000$ $l mol^{-1} cm^{-2}$ for OH³⁴). This is much lower than those previously proposed (46.4 $l mol(H_2)^{-1} cm^{-1}$ or 1650 $l mol(H_2)^{-1} cm^{-2}$)¹⁷ for NAMs (orthopyroxene) annealed under reducing conditions, but in agreement with previous measurements on silica (0.26 $l mol(H_2)^{-1} cm^{-1}$)³³. This further highlights the very low infra-red activity of H_2 and therefore the very low detectability of molecular H_2 by spectroscopic methods. This

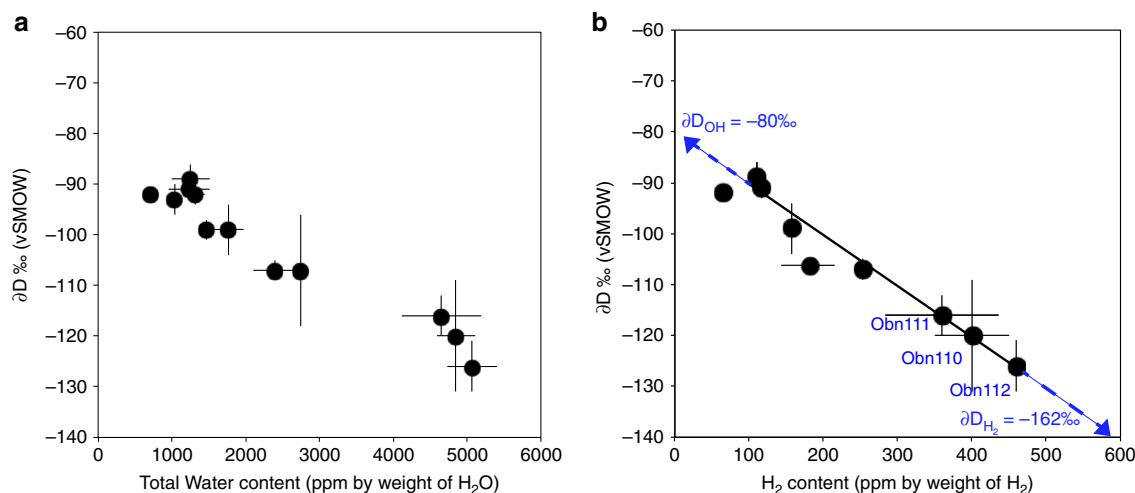


Fig. 3 Hydrogen isotope composition of omphacites versus H content. **a** δD (relative to Vienna Standard Mean Ocean Water - V-SMOW) versus total water content determined by Thermal conversion/Elemental Analyser coupled with Isotope-Ratio Mass spectrometer (TC/EA-IRMS), and **b** δD (relative to V-SMOW) versus calculated H₂ content (wt ppm). Error bars correspond to 1SD.

strongly suggests that the amounts of H determined in previously studied mantle xenoliths have been greatly underestimated.

H isotopic composition. We examine the effects of hydrogen speciation in minerals on H isotope fractionation in the deep water cycle. The δD values in the omphacites from this study correlate well with H concentrations expressed either as H₂O or as H₂ (Fig. 3a, b). The well-defined trend indicates an increase of the δD values in the omphacites with decreasing water content. To confirm the speciation of H, Obnazhennaya samples were heated under vacuum (10^{-3} mbar) at 400 °C, with sample Obn112 incrementally heated at 250, 400, 500, and 600 °C. After each heating step, that lasted 20 min, the samples were re-analysed with FTIR and TC-EA/IRMS. These stepwise experiments show that (1) the bulk water content and the isotopic composition of the samples are little affected by heating up to 400 °C (see Supplementary Table 2). Only two samples (Obn110 and Obn108) suffered up to 15% water loss during heating up to 400 °C. This means that if any inclusions were present, the amount of water stored in them must be negligible or within 15% because otherwise, like in fluid inclusion studies, or for garnets containing water-inclusions, the speciation and concentration of bulk water would be affected^{31,35}. If we consider only the samples annealed at the highest temperature and consider them as the most free of the contribution from inclusions then we get an absorptivity coefficient of $30 \text{ l mol(H}_2\text{)}^{-1} \text{ cm}^{-2}$, instead of the average of $44 \text{ l mol(H}_2\text{)}^{-1} \text{ cm}^{-2}$ determined on the samples before heating at high temperature. (2) Incremental heating of sample Obn112 up to 600 °C yields an increase in the δD values of residual H along with a decrease in OH and H₂ concentrations in omphacite (Fig. 4), in agreement with the general trend described/recorded by the samples. One way to explain this negative correlation between the concentration of total water and isotopic composition is by loss during heating of a component with more negative δD values, such as H₂ or a mixture of H₂ and OH³⁶. Indeed, the global partitioning of H₂ and OH between mineral and fluid would enrich the fluid in ¹H and the residual solid in ²D³⁶. Previous reports of such negative correlation on eclogites from Dabie Sulu have been interpreted by the loss of isotopically light molecular water due to kinetic fractionation of H-D during dehydration in the course of exhumation³⁷. Given that the ascent of kimberlites is very fast, we propose instead that the H-D isotopic fractionation is controlled by the presence of H₂.

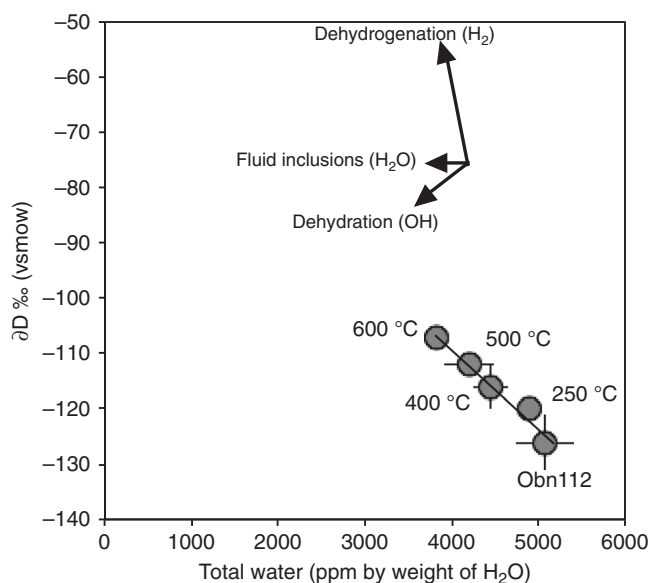
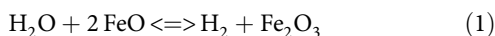


Fig. 4 δD versus H₂O for heated and unheated omphacite Obn112. Total water content (determined by Thermal conversion/Elemental Analyser coupled with Isotope-Ratio Mass spectrometer - TC/EA-IRMS) and δD (relative to Vienna Standard Mean Ocean Water - V-SMOW) show a robust linear correlation. The loss of H with increasing temperature implies higher δD values supporting the loss of a component with much more negative δD (thus H₂ rather than OH or H₂O), as also observed in the infrared spectra where the integrated absorbance of the H₂ band decreases significantly with increasing temperature.

Structural H₂ is indeed observed in omphacite, and the linear relationship between the absorbance of the 4100 cm^{-1} band and the calculated H₂ content indicates that its quantification is robust (see Supplementary Fig. 1). Molecular water present in nano-inclusions seems to be negligible in these samples. However, if present in large quantities, nano-inclusions could also be filled with H₂ given that the conditions of equilibration of the present eclogites are very close to the conditions where H₂ and H₂O are miscible within the mantle³⁸.

As shown in Fig. 2, the absorbance of the 4100 cm^{-1} band decreases with increasing temperature. This decrease is decoupled

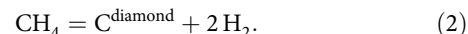
from that of the band at $\sim 4500\text{ cm}^{-1}$ (assigned unambiguously to a Si-OH vibration) implying that these two bands cannot be attributed to the same species, i.e. the 4100 cm^{-1} band is not the result of some combination of OH mode (see Supplementary Figs. 2, 3). Indeed, if these two bands were due to the same species the ratio of their intensities would stay constant, which is not the case: it varies depending on temperature (see Supplementary Fig. 3). While the integrated absorbance of the band at 4500 cm^{-1} decreases, between 100 and $400\text{ }^\circ\text{C}$, that of the 4100 cm^{-1} band increases (Supplementary Fig. 2). This translates into H_2 being produced while OH is being consumed. Thus, we interpret the contrasting behaviour shown in Supplementary Figs. 2, 3 as a transition from OH to H_2 during the heating stage at low temperatures following the oxidation-dehydrogenation shown in reaction 1, similar to what is inferred for natural or experimental samples^{16,39,40}.



Such behaviour also indicates that the kinetics of H_2 and H^+ diffusion are close in this temperature range and cross over at higher temperatures in agreement with previous measurements^{41–44} (Fig. 5).

Reaction 1 is probably responsible for the stabilisation of H_2 in NAMs linked to a change in iron valence in ferro-magnesian silicates, via reduction of water by ferrous iron. Ferric iron solubility increases in clinopyroxene and garnet with increasing pressure¹⁵. Thus, we can expect that eclogitic clinopyroxenes containing 7000–16000 wt ppm Fe, with $\text{Fe}^{3+}/\Sigma\text{Fe}$ estimated at 20–30% due to a high jadeite component [$\text{Na}^+(\text{Al}^{3+}\text{Fe}^{3+})\text{Si}^{4+}_2\text{O}^{2-}_6$]⁴⁵, can easily incorporate the H_2 concentrations measured in this study via reaction 1. Such a reaction is common for dehydration metamorphism in subduction zones³⁹. In the absence of available oxygen, another reaction producing H_2 has

been proposed for the formation of diamond in the cratonic mantle:



However, the preservation within the mantle of high amounts of H (>2000 ppm), considered highly mobile, at high temperatures and for a long time, needs to be explained. Diffusivity of H_2 in minerals is currently unknown but existing data for silicate glasses indicate that H_2 diffusion is not very fast, no faster than for H^+ at mantle conditions. For example, the diffusivity of H_2 in silica glass^{43,44} is $9.3 \times 10^{-16}\text{ m}^2\text{ s}^{-1}$ at $23\text{ }^\circ\text{C}$ and $2.4 \times 10^{-12}\text{ m}^2\text{ s}^{-1}$ at $250\text{ }^\circ\text{C}$. Using the activation energy of 44 kJ mol^{-1} provided in these studies we calculate a diffusivity of H_2 of $1.5 \times 10^{-10}\text{ m}^2\text{ s}^{-1}$ at $600\text{ }^\circ\text{C}$ or $1.0 \times 10^{-9}\text{ m}^2\text{ s}^{-1}$ at $1000\text{ }^\circ\text{C}$ (Fig. 5). Such values are very similar to those determined for the rate of the oxidation reaction⁴⁶ as well as for OH diffusivity in olivine⁴¹ or diopside⁴². The validity of these estimates ultimately hinges on the knowledge of diffusion mechanisms for molecular H_2 in minerals (vacancy vs. interstitial diffusion, polaron or Franck-Turbull mechanisms), which are currently unknown. Considering that H_2 diffusivity experiments in silicate glass have shown a strong dependence (three orders of magnitude)⁴⁶ (Fig. 5) on H_2 partial pressure, the above diffusivity (hence H loss) estimates are likely to be exaggerated. Such diffusivity also implies that equilibrium is geologically fast at the mineral grain scale at moderate to high temperatures, yet high H concentrations could be maintained on the scale of oceanic crust fragments hundreds of metres or kilometres in size. If such eclogitic blocks are preserved for several Ga in the mantle, they will develop hydrogen zoning in terms of abundance and isotope ratios, reflecting their progressive re-equilibration with the ambient mantle.

The surface water cycle fractionates hydrogen isotopes, creating a wide range of isotopically distinct reservoirs, such as Greenland ice caps standard precipitation [$\delta\text{D} = -190\text{‰}$], seawater [VSMOW $\delta\text{D} \sim 0\text{‰}$] and rainwater [$\delta\text{D} = 0\text{--}130\text{‰}$]. The deep water cycle may fractionate hydrogen isotopes as well, but the processes involved are different. Upper mantle (MORB) magmas typically have uniform δD values of $-60 \pm 5\text{‰}$ ⁴⁷, whereas oceanic island magmas, thought to come from the lower mantle, may have much lower δD down to -218‰ ⁴⁸. The δD values for omphacites in this study range from -89 to -126‰ ; they are similar to those reported for orogenic eclogites from the ultra-high pressure (UHP) Sulu terrane (-82 to -128‰ ¹⁸), and lower than those for MORB-like sources ($-60\text{‰} \pm 5$)⁴⁷. Both in our study and previous reports of analyses of UHP rocks by TC/EA-IRMS, the isotopic composition of H is observed to increase with decreasing bulk H of omphacite. This contradicts previous inferences that δD decreases during subduction, hence with dehydration, typically from modern oceanic crustal segments with δD of $-35 \pm 15\text{‰}$ ^{49–51}, to orogenic or cratonic eclogites (remnants of ancient subducted oceanic crust), with δD of -82 to -128‰ ¹⁸. Experimentally determined mineral-water H isotope fractionation factors are generally negative^{52,53} implying that the hydrogen remaining in the slab becomes increasingly depleted in deuterium which preferentially partitions into expelled fluids. Subduction-related dehydration thus causes a decrease in δD in slab materials with depth⁵⁴, as modelled in Fig. 6 (blue trend). The overall mineral-fluid H isotope fractionation factor is difficult to estimate because it varies greatly depending on temperature, pressure and mineral species during subduction-related slab metamorphism. Nevertheless, known H-D isotope fractionation between water and common hydrous minerals (serpentine, amphibole, chlorite, epidote, zoisite, brucite, and clays) range from -10 and -77‰ in the $100\text{--}800\text{ }^\circ\text{C}$ temperature range, with decreasing fractionation at higher temperatures. However, is dehydration the actual process taking place in the present

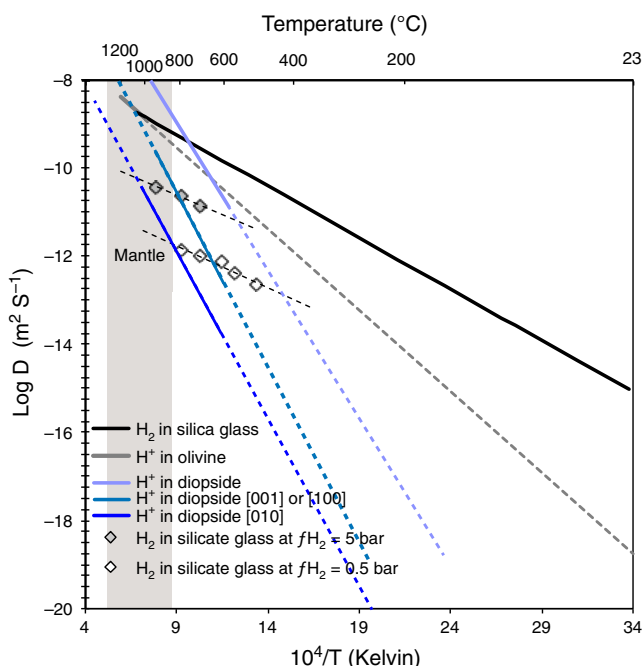


Fig. 5 Experimental diffusivity of H in silicate materials. Diffusivity of hydrogen in silica glass^{43,44}, effective diffusivity in olivine⁴¹, diffusivity in diopside as a function of crystallographic orientation⁴², and the effect of H_2 partial pressure on diffusivity in glass⁴⁶. The grey field corresponds to the temperature range of the lithospheric mantle (dashed lines correspond to low temperature extrapolation of experimental data).

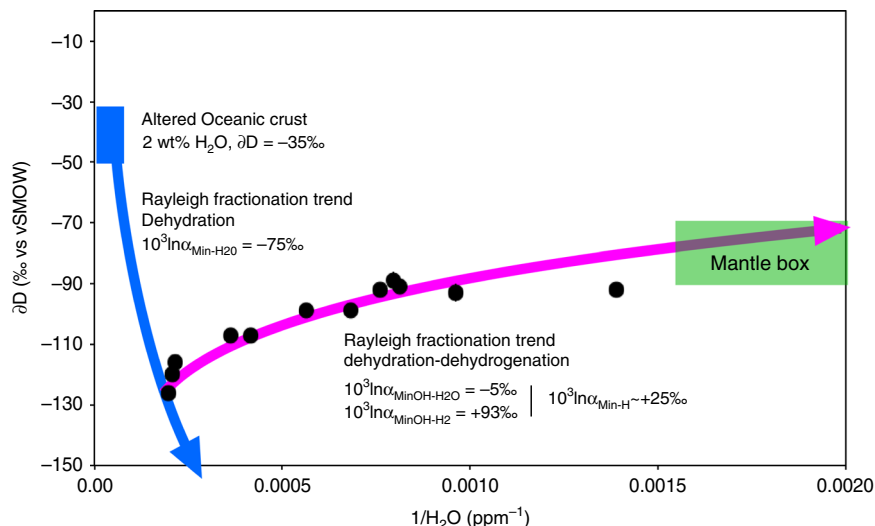


Fig. 6 Model for evolution of H content and δD in mantle omphacites. Hydrogen isotope composition (δD relative to Vienna Standard Mean Ocean Water—V-SMOW) versus $1/H_2O$ (water content determined by Thermal Conversion /Elemental Analyser coupled with Isotope Ratio Mass Spectrometer—TC/EA-IRMS). The blue trend models the compositional evolution of subducting oceanic crust dominated by dehydration. The magenta trend models the compositional evolution of oceanic material, during or post-subduction, dominated by dehydrogenation and dehydration. The model is based on Rayleigh fractionation. The blue box corresponds to the typical isotopic composition of oceanic crust altered by seawater^{55,56} and the green box to the “normal” mantle values⁴⁷.

samples? In this work, we propose that dehydrogenation plays an important role in the isotopic compositions observed (see Fig. 6, green trend).

Here we model the change in the D/H ratio of altered oceanic crust (starting at 2 wt% H_2O , $\delta D = -35\text{‰}$ ^{55,56}) during subduction as it dehydrates. By using a Rayleigh fractionation process and a calculated fractionation factor⁵⁴ ($\alpha_{\text{Mineral-H}_2O} = 0.9277$), it is possible to account for the highest water abundances and the highly negative δD values, observed here for the cratonic omphacites ($[H_2O] = 5065$ ppm, $\delta D = -126\text{‰}$) (Table 1). However, such a low fractionation factor cannot explain why the δD values increase upon dehydration from 5000 to 700 ppm water (Fig. 3a). The enrichment of a mineral in 2D concomitant with dehydration can only be explained if the mineral-fluid fractionation factor is positive, which is the case for H partitioning between minerals and H_2 ³⁶. In such a case, the de-volatilisation is accompanied by the release of a H_2 fluid enriched in 1H instead of a H_2O fluid enriched in 2D , which leads to less negative δD values of residual hydrogen in the mineral. Since the isotope fractionation factor for molecular H_2 is positive and high⁵⁷, extraction of H_2 results in a positive mineral-(OH- H_2) fractionation factor at high temperatures such that δD values of the eclogite become less negative (Figs. 6, 7). Nonetheless, these isotopic compositions cannot be explained by H_2 release alone, which would induce a much faster isotopic evolution. The most likely scenario is a combination of dehydration and dehydrogenation processes (Figs. 6, 7) by diffusion during the very long residence time in the mantle of these eclogitic units as H_2 and H^+ have similar diffusivities at mantle temperature (Fig. 5).

The studied samples show a very good linear correlation between the calculated molecular H_2 content and δD values of total H (R^2 of 0.93, $n = 12$, $p < 0.001$; Fig. 3b). This correlation between H_2 concentration and isotopic composition indicates that the δD in omphacites reflects a mixture of two components, OH and molecular H_2 , each having distinct isotopic compositions. From the proportions of molecular H_2 and the respective isotopic ratios of each sample, it is possible to determine the isotopic compositions of each end-member: $\delta D_{\text{MineralOH}} = -80\text{‰}$ and $\delta D_{\text{MineralH}_2} =$

-162‰ . We can then calculate the intra-mineral fractionation factor between OH and H_2 for the Obnazhennaya omphacites as follows: $\alpha_{\text{MineralOH-MineralH}_2} = 1.098$ ($10^3 \ln \alpha_{\text{MineralOH-MineralH}_2} = +93\text{‰}$). Because hydrogen isotope fractionation between the structurally bound OH (MineralOH) and structurally bound H_2 (Mineral H_2) is $>20\text{‰}$, the fractionation factor was calculated as follows: $\alpha_{A-B} = (1000 + \delta D_A)/(1000 + \delta D_B)$ ⁵³. The intra-mineral fractionation between OH and H_2 calculated here is equivalent to the fractionation between molecular water and molecular hydrogen ($10^3 \ln \alpha_{H_2O-H_2}$: $\sim +100\text{‰}$) at very high temperature (≥ 1100 °C⁵⁷). This suggests that high temperature isotopic equilibrium was reached and preserved in our samples. The diffusive loss of H during the transport of mantle xenoliths close to the surface by kimberlitic magma is low because the magma ascent is very fast⁵⁸.

Since molecular H_2 is most likely to be the dominant form of H in the reduced deep mantle (refs. 3,17), it follows that isotopic fractionation of H in the mantle should be controlled by equilibria involving H_2 -bearing minerals rather than H_2O - or OH-bearing minerals. This must be taken into account when interpreting the H isotopic distribution in the mantle and models involving deep mantle volatile loss⁵⁹. Similar to findings of this study, clinopyroxene (augite) megacrysts from alkaline basalts at Nushan²⁸ yield different H_2O contents by FTIR and TC/EA-IRMS (or manometrically), which correlate negatively with measured δD (see Supplementary Table 1 and Supplementary Fig. 4). Assuming that the measured concentration difference is due to molecular H_2 , the calculated $10^3 \ln \alpha_{\text{MineralOH-MineralH}_2}$ is estimated to be $+111\text{‰}$, which is realistic at magmatic temperatures. In addition, the presence of structurally bound H_2 could explain the large difference in δD values of coexisting richterites (-132‰ vSMOW) and phlogopites (-65‰ vSMOW) in MARID xenolith suites from South African kimberlites, which was previously interpreted as a result of fractional crystallisation or re-equilibration during ascent⁶⁰. Also, a recent discovery of highly negative δD in deep magmas trapped in melt inclusions (e.g.⁴⁸) could be due to different $H_2O_{\text{tot}}-H_2$ proportions and isotopic fractionation controlled by fO_2 ⁶¹ or H_2 loss by diffusion, rather than a primary composition as previously believed. An

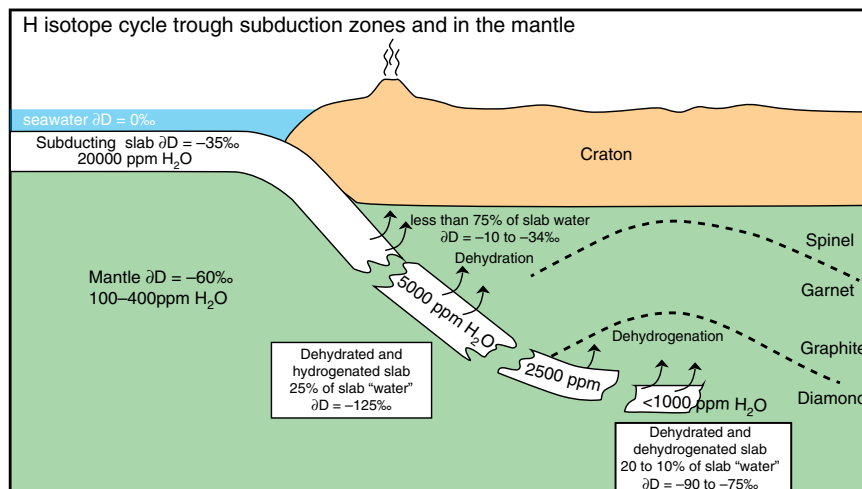


Fig. 7 H recycling and isotope evolution in subduction zone. The sketch shows how the recycled crust gets enriched in ^1H during subduction due to dehydration and subsequently gets enriched in D due to $\text{H}_2\text{-OH}$ equilibration and diffusion within the upper mantle.

accurate determination of H speciation in mantle samples, allowing the quantification of hydrogen in molecular and hydroxyl forms, is therefore a prerequisite for any isotopic measurement and interpretation.

In this study we provide three main pieces of evidence for H_2 in minerals: (i) the discrepancy between hydrogen contents from mass spectrometry and FTIR, (ii) the presence of an absorption band in the infra-red spectra at 4100 cm^{-1} , which scales with the H_2 content, (iii) the isotopic data indicating a preferred partitioning of ^1H into the fluid during H loss. Still, further experimental work is needed to constrain the speciation and mobility of H_2 in mantle minerals and test the model presented here.

Methods

Water content and stable H isotopes determination

“On-line” procedure. Samples were analysed using a continuous flow elemental analyser (TC/EA) operating on-line with mass spectrometer^{19,20,31}. The system used is a ThermoFisher HTFlash IRMS[®] working on-line with DeltaV+[®] mass spectrometer monitored by ConflowIV[®] diluter hosted at the Magmas and Volcanoes laboratory from Université Jean Monnet, Saint-Etienne. The DeltaV+[®] used an electrostatic filter to prevent isobaric interferences between the helium carrier gas and the generated mass 3 of hydrogen. The elemental analyses used the pyrolysis line consisting of a glassy carbon tube filled with glassy carbon grains placed inside an alumina ceramic tube heated at 1450 °C and flushed by helium (100 ml min^{-1}). All hydrogenous gasses were reduced by glassy carbon, H_2 was separated from other gas species (CO) in a chromatographic column heated at 90 °C and transferred to mass spectrometer. ConflowIV[®] diluter monitored the flux and the two injections of H_2 reference gas manufactured by Air Liquid company. The duration of a complete analysis was 300 s. Aliquots of minerals weighting between 0.3 and 25 mg, depending on H_2O content, were analysed. Samples were crushed to fine grains as suggested by^{31,62} to prevent incomplete extraction and fractionation of H and D. All samples were preheated at 100 °C for 24 h to eliminate adsorption water on sample surfaces.

To estimate the impact of tiny fluid inclusions on water content and the role of molecular H_2 on δD , four samples experimented heating. 400 mg of pure handpicked omphacite with grain size ranging between 500 and $1000\text{ }\mu\text{m}$ were put in a 6 mm tube of fused quartz and connected to a vacuum preparation line (10^{-3} mbar). Each sample was held under vacuum and heated with a heat gun by steps of 20 min at 250, 400, 500, and 600 °C . Between each step, an aliquot is taken for FTIR and TC/EA-IRMS analyses.

The relation between hydrogen contents and peak area detected by mass spectrometer was calibrated with benzoic acid (4.952 wt% H), and water concentrations were determined by mass H_2 peak area, the uncertainty is estimated to be $\pm 0.05\text{ wt\%}$.

We have also investigated/addressed linearity issues by loading 36 aliquots of Biotite NBS30 of different weights (0.318–3.423 mg) and thus obtaining different peak sizes on mass 2 (amplitude) in the range of 741 mV to 9396 mV. At the beginning of each analytical session we applied the H_3^+ correction factor at different pressures of the reference gas to correct for different peak heights.

D/H measurements were calibrated against NBS30 biotite and IAEA CH7 polyethylene and previously measured amphibole and mica on VSMOW-GISP isotope scale⁶³ by modified off-line method of⁶⁴ (see below). These have been chosen based on their extremely different δD values (Amphibole AJE 282: $\delta\text{D} = -130 \pm 0.5\text{ ‰}$ and Mica AJE361 $\delta\text{D} = -40 \pm 3\text{ ‰}$ vs VSMOW) spanning over a range of 90% and overlapping with the range of unknown samples. A mean δD value for the NBS30 biotite standard of $-65.4 \pm 1\text{ ‰}$ and water content of $3.67 \pm 0.12\text{ wt\%}$ ($n = 36$) were obtained during the course of this study.

“Off-line” procedure. A suite of amphibole (richterite) and mica (phlogopite) from the South African MARID suite was first analysed using an “off-line” vacuum extraction line. 30–80 mg of pure hand-picked mica and amphibole with grain size ranging between 100 and $200\text{ }\mu\text{m}$ were put in a 6 mm tube of fused quartz and connected to a vacuum preparation line (10^{-9} mbar). Each sample was held at $150\text{--}200\text{ °C}$ for 1 h under vacuum to desorb atmospheric water, and heated gradually with a butane-oxygen torch to release all hydrogenous gas to reach the melting point of quartz tube ($1700\text{--}1800\text{ °C}$). On the line, a CuO grain furnace constantly held at 575 °C allowed to transform all hydrogenous gas to H_2O that was subsequently collected at liquid nitrogen temperature in a 10 mm pyrex cold finger. The trap temperature was increased to -90 °C with a mixture of ethanol-liquid nitrogen to allow the non-condensable gases to be pumped away. Then the collected H_2O was reduced to H_2 with U metal at 800 °C ⁶⁴. H_2 was trapped into a coconut charcoal cold finger at liquid nitrogen temperature and expanded at room temperature in a calibrated volume connected to a capacitance gauge allowing to measure the “total water” content of minerals. On the same line, water standards (IAEA VSMOW, GISP and lab standards) were converted to H_2 with the same procedure. The D/H ratios were determined using an Elemental Isoprime dual-inlet mass spectrometer at the Magmas and Volcanoes laboratory, Jean Monnet University, Saint-Etienne. The results are expressed in the δ -notation as permil relative to VSMOW. A mean δD value for the IAEA NBS30 biotite standard of $-65.7 \pm 0.3\text{ ‰}$ and water content of $3.68 \pm 0.1\text{ wt\%}$ ($n = 4$) were obtained during the course of this study.

FTIR. Ten grains of each sample were doubly polished with final thicknesses of $150\text{--}450\text{ }\mu\text{m}$ depending on the grains. The OH content has been determined on a Bruker Vertex 70 FTIR (Fourier transform infra-red spectroscope) coupled with a Hyperion microscope equipped with $\times 15$ objective and condenser at LMV. Beam size in the analyses varied from 30 to $50\text{ }\mu\text{m}$. The spectra were collected through a CaF_2 plate with a resolution of 2 cm^{-1} and with up to 300 scans. After the application of a linear baseline with anchor points outside the OH stretching region, the absorbance was integrated from 3000 to 3800 cm^{-1} and the absorbance coefficient for omphacite was applied³⁴. The calculation of the water concentration was performed using the Beer-Lambert law: $A = \epsilon \cdot C \cdot t$, where A is the absorbance, ϵ is the absorptivity, C the concentration and t the thickness (in cm). Quantification was based on the average of ~ 10 unpolarised measurements performed on randomly oriented grains within the doubly polished thin sections. The absolute absorbance of the crystal is then equal to three times the unpolarised value as demonstrated by⁶⁵. Absorbances of molecular H_2 and H_2O followed the same procedure and were integrated respectively from 4000 to 4300 cm^{-1} and around 5200 cm^{-1} . The concentration of molecular water was calculated using previously published absorptivity²⁸. The absorptivity of H_2 was calculated using the Beer-Lambert law and the concentrations calculated in Table 1 from the difference

between the total water content measured by TC-EA-IRMS and the water content measured by FTIR in the OH+H₂O frequency region (see Supplementary Fig. 1).

SIMS. In situ water contents were measured on polished sections, gold coated, with the Cameca IMS1280 HR ion microprobe at CRPG-CNRS, Nancy. A 13 kV, 5 nA O⁻ primary beam was focused onto the sample to a diameter of 20 μm. The secondary beam mass resolution was set at 1600, with an energy window of 35 eV and no energy filtering. Secondary ions of H⁺ and D⁺ were measured by peak switching for 10 min by ion counting. Under these analytical conditions, counting rates on H⁺ varied between 1 × 10⁵ and 5 × 10⁵ counts per second and statistical precision ranged from 0.5 to 3%. Samples were carefully degassed before introduction in the analytical chamber. The samples were doubly polished thin sections that were glued on a glass plate and gold coated. They were introduced in the vacuum chamber of the SIMS the night prior to analysis at 2 μPa (2 × 10⁻⁹ atm) associated with a liquid N₂ cold trap. A presputtering of 3 min with a 20 μm raster was used to clean the sample surface before measurement, and a raster of 5 μm and an electronic gate of 90% was used for the analysis. The background level was lower than 10 ppm of water. The water content of samples was calculated by comparing the measured hydrogen secondary ion intensity relative to the primary ion beam intensity of samples with that of pyroxene of known composition⁶⁶ measured during the same session as reference material. The estimated precision on the calculated water content was about 15% (1 sigma). All hydrogen signal is converted into water content, without considering its initial form.

2-Pressure-temperature estimates. Temperatures were calculated with a pressure-dependent garnet-clinopyroxene Fe-Mg geothermometer⁶⁷ for 1, 3, and 7 GPa. Pressures were calculated by projecting the temperature estimates to local conductive model geotherms⁶⁸ corresponding to a surface heat flow of 39 mW m⁻² for Roberts Victor⁶⁹ and of 45 mW m⁻² for Obnazhennaya (estimated at 40 to >50 mW m⁻²)⁷⁰.

Data availability

All data in this study are presented in Table 1 and available in Supplementary Tables 1 and 2.

Received: 4 September 2019; Accepted: 26 June 2020;

Published online: 17 July 2020

References

- Clesi, V. et al. Effect of H₂O on metal-silicate partitioning of Ni, Co, V, Cr, Mn and Fe: implications for the oxidation state of the Earth and Mars. *Geochim. Cosmochim. Acta* **192**, 97–121, <https://doi.org/10.1016/j.gca.2016.07.029> (2016).
- Füri, E., Deloule, E., Gurenko, A. & Marty, B. New evidence for chondritic lunar water from combined D/H and noble gas analyses of single Apollo 17 volcanic glasses. *Icarus* **229**, 109–120, <https://doi.org/10.1016/j.icarus.2013.10.029> (2014).
- Hirschmann, M. M., Withers, A. C., Ardia, P. & Foley, N. T. Solubility of molecular hydrogen in silicate melts and consequences for volatile evolution of terrestrial planets. *Earth Planet. Sci. Lett.* **345–348**, 38–48, <https://doi.org/10.1016/j.epsl.2012.06.031> (2012).
- Peslier, A. H., Schönbächler, M., Busemann, H. & Karato, S.-I. Water in the Earth's interior: distribution and origin. *Space Sci. Rev.* **210**, 1–68 (2017).
- Jacobsen, S. D. Effect of water on the equation of state of nominally anhydrous minerals. *Rev. Mineral. Geochem.* **62**, 321–342, <https://doi.org/10.2138/rmg.2006.62.14> (2006).
- Marty, B. The origins and concentrations of water, carbon, nitrogen and noble gases on Earth. *Earth Planet. Sci. Lett.* **313–314**, 56–66, <https://doi.org/10.1016/j.epsl.2011.10.040> (2012).
- Férot, A. & Bolfan-Casanova, N. Water storage capacity in olivine and pyroxene to 14 GPa: implications for the water content of the Earth's upper mantle and nature of seismic discontinuities. *Earth Planet. Sci. Lett.* **349–350**, 218–230, <https://doi.org/10.1016/j.epsl.2012.06.022> (2012).
- Smyth, J. R. Hydrogen in high pressure silicate and oxide mineral structures. *Rev. Mineral. Geochem.* **62**, 85–115, <https://doi.org/10.2138/rmg.2006.62.5> (2006).
- Bell, D. R. & Rossman, G. R. Water in Earth's mantle: the role of nominally anhydrous minerals. *Science* **255**, 1391 (1992).
- Demouchy, S. & Bolfan-Casanova, N. Distribution and transport of hydrogen in the lithospheric mantle: a review. *Lithos* **240–243**, 402–425, <https://doi.org/10.1016/j.lithos.2015.11.012> (2016).
- Pearson, D. G. et al. Hydrous mantle transition zone indicated by ringwoodite included within diamond. *Nature* **507**, 221, <https://doi.org/10.1038/nature13080> (2014).
- Aulbach, S. et al. Evidence for a dominantly reducing Archaean ambient mantle from two redox proxies, and low oxygen fugacity of deeply subducted oceanic crust. *Sci. Rep.* **9**, 20190, <https://doi.org/10.1038/s41598-019-55743-1> (2019).
- Goncharov, A. G., Ionov, D. A., Doucet, L. S. & Pokhilenko, L. N. Thermal state, oxygen fugacity and COH fluid speciation in cratonic lithospheric mantle: new data on peridotite xenoliths from the Udachnaya kimberlite, Siberia. *Earth Planet. Sci. Lett.* **357–358**, 99–110, <https://doi.org/10.1016/j.epsl.2012.09.016> (2012).
- Woodland, A. B. & Koch, M. Variation in oxygen fugacity with depth in the upper mantle beneath the Kaapvaal craton, Southern Africa. *Earth Planet. Sci. Lett.* **214**, 295–310, [https://doi.org/10.1016/S0012-821X\(03\)00379-0](https://doi.org/10.1016/S0012-821X(03)00379-0) (2003).
- McCammon, C. A. & Frost, D. J. The effect of oxygen fugacity on the olivine to wadsleyite transformation: implications for remote sensing of mantle redox state at the 410 km seismic discontinuity. *Am. Mineral.* **94**, 872–882, <https://doi.org/10.2138/am.2009.3094> (2009).
- Yang, X. Effect of oxygen fugacity on OH dissolution in olivine under peridotite-saturated conditions: an experimental study at 1.5–7 GPa and 1100–1300 °C. *Geochim. Cosmochim. Acta* **173**, 319–336, <https://doi.org/10.1016/j.gca.2015.11.007> (2016).
- Yang, X., Keppler, H. & Li, Y. Molecular hydrogen in mantle minerals. *Geochem. Perspect. Lett.*, 160–168, <https://doi.org/10.7185/geochemlet.1616> (2016).
- Radu, I. B., Harris, C., Moine, B. N., Costin, G. & Cottin, J. Y. Subduction relics in the subcontinental lithospheric mantle, evidence from δ18O variations in eclogite xenoliths from the Kaapvaal craton. *Contrib. Miner. Petrol.* **174**, <https://doi.org/10.1007/s00410-019-1552-z> (2019).
- Gong, B., Zheng, Y.-F. & Chen, R.-X. An online method combining a thermal conversion elemental analyzer with isotope ratio mass spectrometry for the determination of hydrogen isotope composition and water concentration in geological samples. *Rapid Commun. Mass Spectrom.* **21**, 1386–1392, <https://doi.org/10.1002/rcm.2973> (2007).
- Sharp, Z. D., Atudorei, V. & Durakiewicz, T. A rapid method for determination of hydrogen and oxygen isotope ratios from water and hydrous minerals. *Chem. Geol.* **178**, 197–210, [https://doi.org/10.1016/S0009-2541\(01\)00262-5](https://doi.org/10.1016/S0009-2541(01)00262-5) (2001).
- Chen, R.-X., Zheng, Y.-F. & Gong, B. Mineral hydrogen isotopes and water contents in ultrahigh-pressure metabasite and metagranite: constraints on fluid flow during continental subduction-zone metamorphism. *Chem. Geol.* **281**, 103–124, <https://doi.org/10.1016/j.chemgeo.2010.12.002> (2011).
- Katayama, I., Nakashima, S. & Yurimoto, H. Water content in natural eclogite and implication for water transport into the deep upper mantle. *Lithos* **86**, 245–259, <https://doi.org/10.1016/j.lithos.2005.06.006> (2006).
- Smyth, J. R., Bell, D. R. & Rossman, G. R. Incorporation of hydroxyl in upper-mantle clinopyroxenes. *Nature* **351**, 732–735, <https://doi.org/10.1038/351732a0> (1991).
- Doucet, L. S. et al. High water contents in the Siberian cratonic mantle linked to metasomatism: an FTIR study of Udachnaya peridotite xenoliths. *Geochim. Cosmochim. Acta* **137**, 159–187, <https://doi.org/10.1016/j.gca.2014.04.011> (2014).
- Peslier, A. H., Schönbächler, M., Busemann, H. & Karato, S.-I. Water in the Earth's interior: distribution and origin. *Space Sci. Rev.* **212**, 743–810, <https://doi.org/10.1007/s11214-017-0387-z> (2017).
- Allègre, C. J. & Turcotte, D. L. Implications of a two-component marble-cake mantle. *Nature* **323**, 123, <https://doi.org/10.1038/323123a0> (1986).
- Newman, S., Stolper, E. M. & Epstein, S. Measurement of water in rhyolitic glasses; calibration of an infrared spectroscopic technique. *Am. Mineral.* **71**, 1527–1541 (1986).
- Kovács, I. et al. Water concentrations and hydrogen isotope compositions of alkaline basalt-hosted clinopyroxene megacrysts and amphibole clinopyroxenites: the role of structural hydroxyl groups and molecular water. *Contrib. Miner. Petrol.* **171**, <https://doi.org/10.1007/s00410-016-1241-0> (2016).
- Su, W., You, Z., Cong, B., Ye, K. & Zhong, Z. Cluster of water molecules in garnet from ultrahigh-pressure eclogite. *Geology* **30**, 611–614, [https://doi.org/10.1130/0091-7613\(2002\)030<0611:cwmig>2.0.co;2](https://doi.org/10.1130/0091-7613(2002)030<0611:cwmig>2.0.co;2) (2002).
- Xu, Z., Zheng, Y.-F., Zhao, Z.-F. & Gong, B. The hydrous properties of subcontinental lithospheric mantle: constraints from water content and hydrogen isotope composition of phenocrysts from Cenozoic continental basalt in North China. *Geochim. Cosmochim. Acta* **143**, 285–302, <https://doi.org/10.1016/j.gca.2013.12.025> (2014).
- Gong, B., Zheng, Y.-F. & Chen, R.-X. TC-EA-MS online determination of hydrogen isotope composition and water concentration in eclogitic garnet. *Phys. Chem. Miner.* **34**, 687–698, <https://doi.org/10.1007/s00269-007-0184-4> (2007).
- Bartholomew, R. F., Butler, B. L., Hoover, H. L. & Wu, C. K. Infrared spectra of a water-containing glass. *J. Am. Ceram. Soc.* **63**, 481–485, <https://doi.org/10.1111/j.1151-2916.1980.tb10748.x> (1980).

33. Shelby, J. E. Protonic species in vitreous silica. *J. Non-Cryst. Solids* **179**, 138–147 (1994).
34. Koch-Müller, M., Abs-Wurmbach, I., Rhede, D., Kahlenberg, V. & Matsyuk, S. Dehydration experiments on natural omphacites: qualitative and quantitative characterization by various spectroscopic methods. *Phys. Chem. Miner.* **34**, 663–678, <https://doi.org/10.1007/s00269-007-0181-7> (2007).
35. Ishiyama, D., Shinoda, K., Shimizu, T., Matsubaya, O. & Aikawa, N. Structural states and isotopic compositions of water in hydrothermal quartz, Koryu Deposit, Japan. *Econ. Geol.* **94**, 1347–1351, <https://doi.org/10.2113/gsecongeo.94.8.1347> (1999).
36. Vennemann, T. W. & O’Neil, J. R. Hydrogen isotope exchange reactions between hydrous minerals and molecular hydrogen: I. a new approach for the determination of hydrogen isotope fractionation at moderate temperatures. *Geochim. Cosmochim. Acta* **60**, 2437–2451, [https://doi.org/10.1016/0016-7037\(96\)00103-2](https://doi.org/10.1016/0016-7037(96)00103-2) (1996).
37. Sheng, Y.-M. & Gong, B. Hydrous species in eclogitic omphacite: implication for metamorphic dehydration during exhumation. *J. Asian Earth Sci.* **145**, 123–129, <https://doi.org/10.1016/j.jseas.2016.12.020> (2017).
38. Bali, E., Audétat, A. & Keppler, H. Water and hydrogen are immiscible in Earth’s mantle. *Nature* **495**, 220–222, <https://doi.org/10.1038/nature11908> (2013).
39. Plesier, A. H., Luhr, J. F. & Post, J. Low water contents in pyroxenes from spinel-peridotites of the oxidized, sub-arc mantle wedge. *Earth Planet. Sci. Lett.* **201**, 69–86, [https://doi.org/10.1016/S0012-821X\(02\)00663-5](https://doi.org/10.1016/S0012-821X(02)00663-5) (2002).
40. Skogby, H. O. H. incorporation in synthetic clinopyroxene. *Am. Mineral.* **79**, 240–249 (1994).
41. Demouchy, S. Diffusion of hydrogen in olivine grain boundaries and implications for the survival of water-rich zones in the Earth’s mantle. *Earth Planet. Sci. Lett.* **295**, 305–313, <https://doi.org/10.1016/j.epsl.2010.04.019> (2010).
42. Hercule, S. & Ingrin, J. Hydrogen in diopside; diffusion, kinetics of extraction-incorporation, and solubility. *Am. Mineral.* **84**, 1577–1587, <https://doi.org/10.2138/am-1999-1011> (1999).
43. Shang, L., Chou, I. M., Lu, W., Burruss, R. C. & Zhang, Y. Determination of diffusion coefficients of hydrogen in fused silica between 296 and 523K by Raman spectroscopy and application of fused silica capillaries in studying redox reactions. *Geochim. Cosmochim. Acta* **73**, 5435–5443, <https://doi.org/10.1016/j.gca.2009.06.001> (2009).
44. Lee, R. W. Diffusion of hydrogen in natural and synthetic fused quartz. *J. Chem. Phys.* **38**, 448–455, <https://doi.org/10.1063/1.1733679> (1963).
45. Schmid, R. et al. Micro-XANES determination of ferric iron and its application in thermobarometry. *Lithos* **70**, 381–392, [https://doi.org/10.1016/S0024-4937\(03\)00107-5](https://doi.org/10.1016/S0024-4937(03)00107-5) (2003).
46. Gaillard, F., Schmidt, B., Mackwell, S. & McCammon, C. Rate of hydrogen–iron redox exchange in silicate melts and glasses. *Geochim. Cosmochim. Acta* **67**, 2427–2441, [https://doi.org/10.1016/S0016-7037\(02\)01407-2](https://doi.org/10.1016/S0016-7037(02)01407-2) (2003).
47. Clog, M., Aubaud, C., Cartigny, P. & Dosso, L. The hydrogen isotopic composition and water content of southern Pacific MORB: a reassessment of the D/H ratio of the depleted mantle reservoir. *Earth Planet. Sci. Lett.* **381**, 156–165, <https://doi.org/10.1016/j.epsl.2013.08.043> (2013).
48. Hallis, L. J. et al. Evidence for primordial water in Earth’s deep mantle. *Science* **350**, 795 (2015).
49. Satake, H. & Matsuda, J. i. Strontium and hydrogen isotope geochemistry of fresh and metabasalt dredged from the Mid-Atlantic Ridge. *Contrib. Mineral. Petrol.* **70**, 153–157, <https://doi.org/10.1007/BF00374444> (1979).
50. Sheppard, S. M. F. & Epstein, S. D/H and 18O/16O ratios of minerals of possible mantle or lower crustal origin. *Earth Planet. Sci. Lett.* **9**, 232–239 (1970).
51. Wenner, D. B. & Taylor, H. P. D/H and O18/O16 studies of serpentinization of ultramafic rocks. *Geochim. Cosmochim. Acta* **38**, 1255–1286, [https://doi.org/10.1016/0016-7037\(74\)90120-3](https://doi.org/10.1016/0016-7037(74)90120-3) (1974).
52. Graham, C. M., Harmon, R. S. & Sheppard, S. M. F. Experimental hydrogen isotope studies: hydrogen isotope exchange between amphibole and water. *Am. Miner.* **69**, 128–138 (1984).
53. Suzuoki, T. & Epstein, S. Hydrogen isotope fractionation between OH-bearing minerals and water. *Geochim. Cosmochim. Acta* **40**, 1229–1240, [https://doi.org/10.1016/0016-7037\(76\)90158-7](https://doi.org/10.1016/0016-7037(76)90158-7) (1976).
54. Shaw, A. M., Hauri, E. H., Fischer, T. P., Hilton, D. R. & Kelley, K. A. Hydrogen isotopes in Mariana arc melt inclusions: implications for subduction dehydration and the deep-Earth water cycle. *Earth Planet. Sci. Lett.* **275**, 138–145, <https://doi.org/10.1016/j.epsl.2008.08.015> (2008).
55. Ito, E., Harris, D. M. & Anderson, A. T. J. Alteration of oceanic crust and geologic cycling of chlorine and water. *Geochim. Cosmochim. Acta* **47**, 1613–1624 (1983).
56. Peacock, S. M. Fluid processes in subduction zones. *Science* **248**, 329–337 (1990).
57. Richet, P., Bottinga, Y. & Javoy, M. A review of hydrogen, carbon, nitrogen, oxygen, sulphur, and chlorine stable isotope fractionation among gaseous molecules. *Annu. Rev. Earth Planet. Sci.* **5**, 65–110, <https://doi.org/10.1146/annurev.ea.05.050177.000433> (1977).
58. Plesier, A. H., Woodland, A. B. & Wolff, J. A. Fast kimberlite ascent rates estimated from hydrogen diffusion profiles in xenolithic mantle olivines from southern Africa. *Geochim. Cosmochim. Acta* **72**, 2711–2722, <https://doi.org/10.1016/j.gca.2008.03.019> (2008).
59. Sharp, Z. D., McCubbin, F. M. & Shearer, C. K. A hydrogen-based oxidation mechanism relevant to planetary formation. *Earth Planet. Sci. Lett.* **380**, 88–97, <https://doi.org/10.1016/j.epsl.2013.08.015> (2013).
60. Kuroda, Y., Suzuoki, T., Matsuo, S. & Aoki, K. I. D/H ratios of the coexisting phlogopite and richterite from mica nodules and a peridotite in South African kimberlites. *Contrib. Mineral. Petrol.* **52**, 315–318, <https://doi.org/10.1007/BF00401460> (1975).
61. Mysen, B. Hydrogen isotope fractionation and redox-controlled solution mechanisms in silicate-COH melt+fluid systems. *J. Geophys. Res.: Solid Earth* **120**, 7440–7459, <https://doi.org/10.1002/2015JB011954> (2015).
62. Qi, H., Coplen, T. B., Olack, G. A. & Vennemann, T. W. Caution on the use of NBS 30 biotite for hydrogen-isotope measurements with on-line high-temperature conversion systems. *Rapid Commun. Mass Spectrom.* **28**, 1987–1994, <https://doi.org/10.1002/rcm.6983> (2014).
63. Coplen, T. B. Reporting of stable hydrogen, carbon, and oxygen isotopic abundances. *Geothermics* **24**, 707–712, [https://doi.org/10.1016/0375-6505\(95\)00024-0](https://doi.org/10.1016/0375-6505(95)00024-0) (1995).
64. Bigeleisen, J., Perlman, M. L. & Prosser, H. C. Conversion of hydrogenic materials to hydrogen for isotopic analysis. *Anal. Chem.* **24**, 1356–1357 (1952).
65. Kovács, I. N. et al. Quantitative absorbance spectroscopy with unpolarized light: Part II. Experimental evaluation and development of a protocol for quantitative analysis of mineral IR spectra. *Am. Mineral.* **93**, 765–778, <https://doi.org/10.2138/am.2008.2656> (2008).
66. Xia, Q.-K., Dallai, L. & Delouie, E. Oxygen and hydrogen isotope heterogeneity of clinopyroxene megacrysts from Nushan Volcano, SE China. *Chem. Geol.* **209**, 137–151, <https://doi.org/10.1016/j.chemgeo.2004.04.028> (2004).
67. Ravna, K. The garnet–clinopyroxene Fe²⁺–Mg geothermometer: an updated calibration. *J. Metamorph. Geol.* **18**, 211–219, <https://doi.org/10.1046/j.1525-1314.2000.00247.x> (2000).
68. Pollack, H. N. & Chapman, D. S. Mantle heat flow. *Earth Planet. Sci. Lett.* **34**, 174–184, [https://doi.org/10.1016/0012-821X\(77\)90002-4](https://doi.org/10.1016/0012-821X(77)90002-4) (1977).
69. Griffin, W., O’Reilly, S. Y., Natapov, L. M. & Ryan, C. G. The evolution of lithospheric mantle beneath the Kalahari Craton and its margins. *Lithos* **71**, 215–241, <https://doi.org/10.1016/j.lithos.2003.07.006> (2003).
70. Ionov, D. A., Doucet, L. S., Xu, Y., Golovin, A. V. & Oleinikov, O. B. Reworking of Archean mantle in the NE Siberian craton by carbonate and silicate melt metasomatism: evidence from a carbonate-bearing, dunite-to-websterite xenolith suite from the Obnazhennaya kimberlite. *Geochim. Cosmochim. Acta* **224**, 132–153, <https://doi.org/10.1016/j.gca.2017.12.028> (2018).

Acknowledgements

This research was supported by the Laboratory of Excellence ClerVolc, Jean Monnet University-Saint-Etienne and CPER AURA. AK, AG, and OO were supported by Russian Federation state assignment projects of IGM SB RAS and of DPMGI SB RAS. This research was financed by the French Government Laboratory of Excellence Initiative n° ANR-10-LABX-0006 and by the TelluS programme of CNRS/INSU. This is Laboratory of Excellence ClerVolc contribution n°415. The authors thank Prof. Chris Harris for discussions and his improvements on the English writing.

Author contributions

B.N.M. performed the H₂O_{tot} and δD measurements (TC/EA-IRMS and off-line/Dual-inlet method). I.B.R., B.N.M., and N.B.-C. performed FTIR measurements, and E.D. performed SIMS measurements. I.B.R. calculated pressure–temperature equilibration conditions. G.C., D.I., A.G., A.K., and O.O. provided the samples. B.N.M., N.B.-C. I.B.R., D.I., J.-Y.C. A.K., A.G., and E.D. contributed ideas, models, plots, and participated in writing of the manuscript. B.N.M. took the lead in preparing the manuscript with input from the other authors.

Competing interests

The authors declare that they have no known competing financial interests or personal relationships that could have appeared to influence the work reported in this paper

Additional information

Supplementary information is available for this paper at <https://doi.org/10.1038/s41467-020-17442-8>.

Correspondence and requests for materials should be addressed to B.N.M.

Peer review information *Nature Communications* thanks Hans Keppler, Xiaozhi Yang and the other, anonymous, reviewer(s) for their contribution to the peer review of this work. Peer reviewer reports are available.

Reprints and permission information is available at <http://www.nature.com/reprints>

Publisher's note Springer Nature remains neutral with regard to jurisdictional claims in published maps and institutional affiliations.



Open Access This article is licensed under a Creative Commons Attribution 4.0 International License, which permits use, sharing, adaptation, distribution and reproduction in any medium or format, as long as you give appropriate credit to the original author(s) and the source, provide a link to the Creative Commons license, and indicate if changes were made. The images or other third party material in this article are included in the article's Creative Commons license, unless indicated otherwise in a credit line to the material. If material is not included in the article's Creative Commons license and your intended use is not permitted by statutory regulation or exceeds the permitted use, you will need to obtain permission directly from the copyright holder. To view a copy of this license, visit <http://creativecommons.org/licenses/by/4.0/>.

© The Author(s) 2020